Physics of Plasmas

Modeling of chirping toroidal Alfvén eigenmodes in NSTX

Cite as: Phys. Plasmas **26**, 092103 (2019); https://doi.org/10.1063/1.5115399
Submitted: 18 June 2019 . Accepted: 17 August 2019 . Published Online: 06 September 2019

R. B. White, V. N. Duarte, N. N. Gorelenkov, E. D. Fredrickson, M. Podestà, and H. L. Berk

Physics of Plasmas ARTICLE scitation.org/journal/php

Modeling of chirping toroidal Alfvén eigenmodes in NSTX

Cite as: Phys. Plasmas **26**, 092103 (2019); doi: 10.1063/1.5115399
Submitted: 18 June 2019 · Accepted: 17 August 2019 ·
Published Online: 6 September 2019

R. B. White,[1,a)] V. N. Duarte,[1] N. N. Gorelenkov,[1] E. D. Fredrickson,[1] M. Podestà,[1] and H. L. Berk[2]

AFFILIATIONS

[1]Princeton Plasma Physics Laboratory, Princeton University, Princeton, New Jersey 08543, USA
[2]Institute for Fusion Studies, University of Texas, Austin, Texas 78712, USA

[a)]Electronic mail: rwhite@pppl.gov

ABSTRACT

Modulation of mode amplitude and frequency of TAE modes, observed experimentally and referred to as chirping, is investigated using a guiding center code and a δf formalism. Chirping is observed as the development in time of Fourier sidebands that move above and below the nominal mode frequency. Subsequent doubling of the sidebands is also sometimes observed. Equilibria with conventional positive magnetic shear are used, as well as NSTX reversed shear cases. The onset of chirping can be triggered by a sudden increase in mode damping, as can occur by the mode contacting the continuum.

https://doi.org/10.1063/1.5115399

I. INTRODUCTION

Complex behavior of Alfvén modes is often observed in tokamak discharges, including rapid frequency changes referred to as chirps, occurring at time scales much shorter than the typical time for changes in the equilibrium. The modeling of chirping has been attracting considerable interest, both in idealized and realistic geometries.[1–14] Aside from being an interesting test of the capability of numerical simulation, the existence of chirping can significantly modify high energy particle distributions. In general, spherical tokamaks exhibit Alfvénic wave chirping more prominently than conventional tokamaks,[15] which has been explained in terms of the reduced relative microturbulence at the ion scale in spherical machines.[16] Alfvénic avalanches, during which a significant fraction of the fast ions is typically lost,[17] are often preceded by a sequence of chirping events. In this work, we examine unstable Alfvén modes with damping a significant fraction of the drive, using the guiding center code Orbit[18] and a delta f formalism to reproduce the chirping behavior. The code, which can use a numerically produced NSTX[19] equilibrium, mode eigenfunctions produced by NOVA,[20] and the numerical beam particle distribution produced by TRANSP,[21] has been described in previous publications.[22–24] The modeling of chirping is a major tool for describing mode-induced fast ion losses in present tokamaks, as well as in ITER, where chirping cannot be ruled out.[25] Because of the strong rotation shear in NSTX, the TAE gap can close, making it easy for a mode to contact the Alfvénic continuum. This provides a sudden increase in the damping rate for the mode, which can act to produce a chirp. Frequency chirping is typically seen in a simulation when large mode damping produces a collapse in the mode amplitude to a small value and consists in the production of a phase space particle clump and hole, diverging above and below from the nominal mode frequency.

The equilibrium magnetic field is given by

$$\vec{B} = h\nabla\zeta + I\nabla\theta + \delta\nabla\psi_p, \tag{1}$$

where θ and ζ are the poloidal and toroidal coordinates, ψ_p is the poloidal flux, and in an axisymmetric equilibrium using Boozer coordinates, h and I are the functions of ψ_p only. The perturbation has the form $\delta\vec{B} = \nabla \times \alpha\vec{B}$, and α and an electric potential Φ have the Fourier expansions,

$$\alpha = \sum_{m,n} A_n \alpha_{m,n}(\psi)\sin(\Omega_{mn}), \quad \Phi = \sum_{m,n} A_n \Phi_{m,n}(\psi)\sin(\Omega_{mn}), \tag{2}$$

where n refers to a single mode with definite toroidal mode number and frequency and the sum is over poloidal harmonics m with $\Omega_{mn} = n\zeta - m\theta - \omega_n t - \phi_n$, in which ϕ_n is the mode phase. For ideal modes, the electric potential Φ is chosen to cancel the parallel electric field induced by $d\vec{B}/dt$, requiring

$$\sum_{m,n} \omega_n B \alpha_{m,n}\cos(\Omega_{mn}) - \vec{B}\cdot\nabla\Phi/B = 0,$$

giving Boozer coordinates

$$(hq + I)\omega_n \alpha_{mn} = (nq - m)\Phi_{mn}.$$

The perturbation α is related to the ideal displacement $\vec{\xi}$, through

$$\alpha_{mn} = \frac{(m/q - n)}{(mh + nI)} \xi^{\psi}_{mn}.$$

The eigenfunctions produced with the code NOVA[20] are normalized with the largest harmonic $\xi^{\psi}_{mn}(\psi_p)$ having a maximum amplitude of 1. Thus, amplitude A_n is the magnitude of the ideal displacement caused by this harmonic, normalized to the major radius R. The perturbed radial magnetic field is approximately given by

$$\frac{\delta B_r}{B} \simeq \frac{mR}{r} A_n. \tag{3}$$

The modification of the particle distribution by the mode is carried out using a delta f formalism. The particle distribution is written as $f = f_0 + \delta f$, where the distribution in the absence of the modes f_0 is a function of E and P_ζ and is independent of time. Following particle orbits $df/dt = 0$ and to order α,

$$\frac{d}{dt}\delta f = -\partial_E f_0 \dot{E} - \partial_{P_\zeta} f_0 \dot{P}_\zeta. \tag{4}$$

The numerically loaded and evolved distribution function is $g(\psi_p, \theta, \zeta, \rho_\parallel, t)$ with $dg/dt = 0$. The distribution g has the Klimontovich representation

$$g(\psi_p, \theta, \zeta, \rho_\parallel, t) = \sum_j \delta(\psi_p - \psi_{p,j}(t))\delta(\theta - \theta_j(t)) \times \delta(\zeta - \zeta_j(t))\delta(\rho_\parallel - \rho_{\parallel,j}), \tag{5}$$

where j is the particle index and δf is represented by

$$\delta f(\psi_p, \theta, \zeta, \rho_\parallel, t) = \sum_j w_j \delta(\psi_p - \psi_{p,j}(t))\delta(\theta - \theta_j(t)) \times \delta(\zeta - \zeta_j(t))\delta(\rho_\parallel - \rho_{\parallel,j}(t)). \tag{6}$$

Defining $w = \delta f/g$ from Eq. (4),

$$dw/dt = -(1/g)df_0/dt = -(f_0/g)dln(f_0)/dt = -(f/g - w)dln(f_0)/dt, \tag{7}$$

and f/g is a constant in time and given by the value at $t = 0$. Normally, simulations assume that the initial perturbation of the distribution δf is zero, and so initially $w(0) = 0$.

Stepping equations for the mode amplitude and phase were previously derived,[22,23]

$$\frac{dA_n}{dt} = \frac{-\nu_A^2}{D_n \omega_n A_n} \sum_{j,m} w_{n,j} \left[\rho_\parallel B^2 \alpha_{mn}(\psi_p) - \Phi_{mn}(\psi_p)\right] \cos(\Omega_{mn}) - \gamma_d A_n, \tag{8}$$

$$\frac{d\phi_n}{dt} = \frac{-\nu_A^2}{D_n \omega_n A_n^2} \sum_{j,m} w_{n,j} \left[\rho_\parallel B^2 \alpha_{mn}(\psi_p) - \Phi_{mn}(\psi_p)\right] \sin(\Omega_{mn}), \tag{9}$$

with $D_n = 4\pi^2 \sum_m \int \xi^2_{mn}(\psi_p) d\psi_p$, j being the particle index, ψ_p, θ, and ζ being the position of particle j, and $\rho_\parallel$ being the normalized parallel velocity. The linear damping rate γ_d is due to the continuum, electron, and thermal ion Landau damping and radiation; all terms in the sums are evaluated at the coordinates of particle j, and $w_{n,j}$ is the δf weight of particle j for mode n.

From these equations, it is clear that there is a much more significant modulation of the mode frequency compared to the mode growth if both the drive and the damping are large. The modified mode frequency is given by $\omega_n + d\phi_n/dt$. Aside from the difference in sine vs cosine, the drive for ϕ_n and A is the same, but the damping diminishes the effect of the drive on the amplitude but not on the frequency.

Analysis of the mode frequency spectrum is done using the Wigner distribution of quasiprobability,[26,27]

$$W(t, \omega_k) = \int_{-T}^{T} \Phi^*(t + q)\Phi(t - q)e^{-2i\omega_k q} dq, \tag{10}$$

where we consider a single mode with frequency ω_n and $\Phi(t) = [\cos(\omega_n t + \phi(t)) + i\sin(\omega_n t + \phi(t))]$. The spectrum given by ω_k is chosen to span the mode frequency with a range large enough to include the chirps. This has advantages over a Fourier analysis with a Gaussian window centered on time t. In particular, if $\Phi = constant$, then in the limit of large T, $W(t, \omega_k) = \delta(\omega_k)/2\pi$. If the mode consists of a single poloidal harmonic $\Phi = e^{-i\omega_n t}$, then $W(t, \omega_k) = \delta(\omega_k - \omega_n)/2\pi$, and if Φ is a single chirp, $\Phi = e^{-i\omega_n t^2/2}$ then $W(t, \omega_k) = \delta(\omega_k - 2\omega_n t)/2\pi$. In addition, W is second order in Φ, and so it gives a stronger resolution of relative amplitudes than a linear Fourier analysis.

Introducing units of time given by ω_0^{-1}, where $\omega_0 = eB_0/(mc)$ is the on axis gyro frequency, and units of distance given by the major radius R_0, the basic unit of energy becomes $m\omega_0^2 R_0^2$, which can also be written as $(mv^2/2)(2R^2/\rho^2)$; the gyro radius is $\rho = v/B \ll 1$, and the magnetic moment $\mu = v_\perp^2/(2B)$ is of order ρ^2.

In Sec. II, we discuss the numerical results from simulations, beginning with an axisymmetric equilibrium with a canonical q profile, quadratic in the minor radius, and a mode with a typical Alfvén frequency of 100 kHz, and then discuss simulations of chirping obtained using numerical NSTX equilibria where chirps were experimentally observed, with negative shear in the plasma core. In Section III is the conclusion.

II. NUMERICAL RESULTS

We have experimented with the range of the spectrum ω_k and the magnitude of the time average T in the analysis of, and the search for, chirping. The results differ significantly by varying these parameters, resulting in greater or lesser clarity of the process. The time step used in the code for these simulations was $dt \simeq 10^{-8}$ s and the mode frequencies were around 100 kHz, and so $\omega dt = 0.01$, sufficiently small to give good cancelation of incoherent rapid time dependence in the integrals. We assume the time dependence of $A(t)$ and $\phi(t)$ to be much slower than ω_k and more on the order of the initial linear growth rate γ_L. We have chosen at least 51 frequencies ω_k spanning a range of frequencies including the nominal mode frequency ω. Typically, the range of frequencies includes up to a 20% change from the mode frequency ω, and the time average T was chosen to be 50 toroidal transit times.

A. A quadratic q profile equilibrium

Initial investigations were with a conventional equilibrium with a q profile quadratic in the minor radius. In Fig. 1 are shown the equilibrium and q profile used. The field on the axis was 4.9 kG.

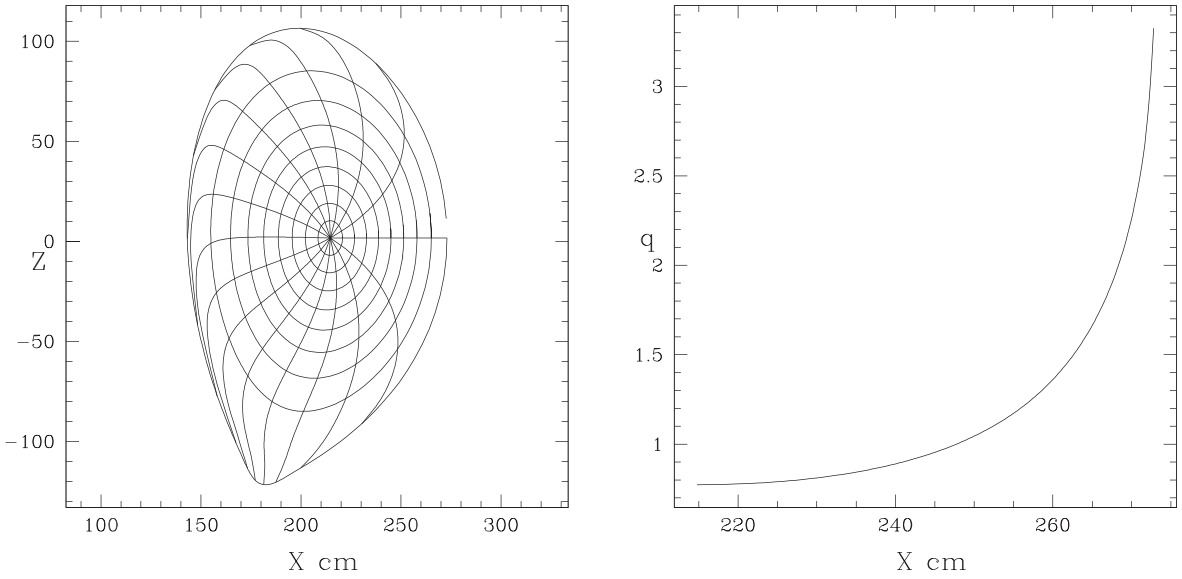

FIG. 1. Equilibrium and helicity profile $q(\psi_p)$.

A perturbation consisting of an ideal mode was used with a single harmonic $\xi(\psi_p)$ with $m = 6$ and $n = 5$, with a simple Gaussian radial profile. There is also an electric potential chosen to cancel the electric field parallel to $\vec{B}$. The use of a single harmonic greatly speeds up the simulation compared to cases with modes of many harmonics. The instability drive was given by a simple local constant gradient in canonical momentum, equivalent to a gradient in minor radius, but a gradient in energy can also be used without changing results.

We find that a simple way to produce a chirp is to initiate a strongly unstable mode with no collisions and strong damping, with the damping reducing the growth to a small fraction of the linear growth rate. The eigenfunction is associated with the unstable mode. Without collisions, the mode grows only until it has flattened the distribution function within the resonance and then abruptly decays due to the damping. The strongly correlated particles in the resonance are then suddenly left without the structure provided by the perturbed field, and as the mode decays, they typically leave by forming a clump and a hole, giving Fourier sidebands both above and below the mode frequency. The direct modification of the particle density is not observable with our existing capabilities because changes in the particle density occur in narrow domains of energy and momentum. What can be observed are the Fourier sidebands departing from the principle mode frequency as the chirp occurs.

The code is initiated with the mode having a small amplitude, $A = 10^{-4}$ or smaller, with different instability strengths and mode damping values. To achieve chirping the linear growth rate γ_L and also the damping, γ_d must be large. We considered primarily cases of collisionless plasmas, but included in some cases also energy drag and collisions. The particle distribution was chosen with a single value of magnetic moment μ, with $\mu B = 2$ keV, deeply passing, conserved in the absence of collisions. From 200 000 to 500 000 particles were used in the simulations. Note that particles on good KAM[28] surfaces cannot exchange energy with the mode except in an adiabatic manner and thus cannot participate in mode growth or chirp formation. Only that part of the distribution associated with the resonance need to be represented. Changing the value of μ modifies the location of the resonance, and thus, including a significant range of μ values would require a much larger distribution. The value of μ is chosen to be characteristic of the particle distribution, and the results are found to be relatively insensitive to this choice. To demonstrate this, we use two very different values of μ for the NSTX cases considered.

The kinetic Poincaré plot of the resonance is shown in Fig. 2, for mode amplitude $A = 10^{-3}$ and $\mu B = 2$ keV. The equilibrium and perturbation were selected[29,30] to give a single well isolated resonance, surrounded by good KAM surfaces in both E and P_ζ. Both the energy distribution and that in canonical momentum were chosen to have several times the width of the largest resonance observed during the simulation. As shown in Fig. 2, the energy of the resonance was about 94 keV.

In Fig. 3 is shown a typical time history of the mode amplitude and growth rate, for a case producing chirping. The mode is initiated at a small amplitude with no collisions or energy drag. It grows due to the initial density gradient within the resonance, but when this free energy supply is exhausted, the large value of damping produces a rapid decay of the mode amplitude. Shown is the linear growth rate γ_L as well as the actual drive of the mode, $\gamma_L - \gamma_d$. When the mode crashes to a low amplitude, the particle distribution in the resonance is restored, and so the mode again grows up to the point of flattening the internal density gradient and the process repeats. As long as the linear growth rate is large, and the damping a significant fraction of this, chirping is observed practically at every amplitude crash although the form of the chirp can vary. Cases with smaller damping fail to chirp even though the amplitude may decay to a small value. The experimental situation is similar, in that what is typically observed is a stable saturated Alfvén mode suddenly experiencing chirping. We have also simulated this scenario, by adjusting collision rates and mode drive to

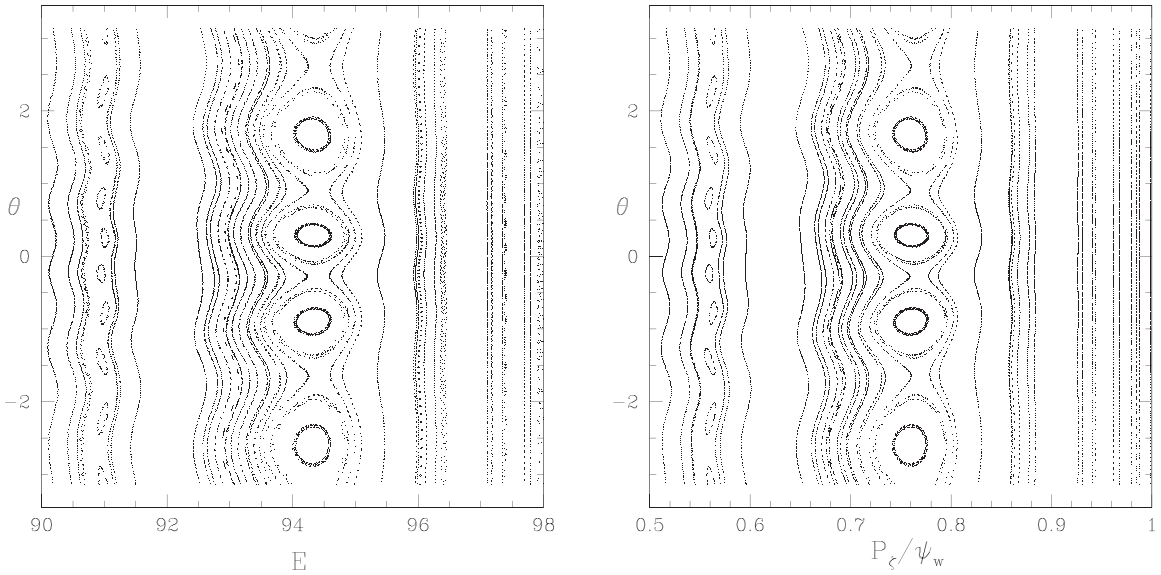

FIG. 2. Kinetic Poincaré plots in canonical momentum and in energy, with $\mu B = 2$ keV, a mode frequency of 100 kHz, and a large mode amplitude of $A = 10^{-3}$. The range of the particle distribution must completely cover the resonance at a maximum amplitude. The resonance has a poloidal structure of four elliptic points.

produce a stable saturated mode and then suddenly increasing the mode damping. The results are the same, but this scenario requires more significant work and time than simply initiating a mode with strong drive and strong damping.

The initial part of the chirp, including the development of the sideband frequencies, is well described by theory. There is no theory capable of describing the full evolution including multiple chirps. The very rapid change of the growth rate from strongly damped to strongly growing at the amplitude minimum is perhaps due to the clump and hole completely replacing the population of the small resonance island at this point, but this is pure conjecture. We have examined the mode phase during the evolution, and there are no strong phase jumps

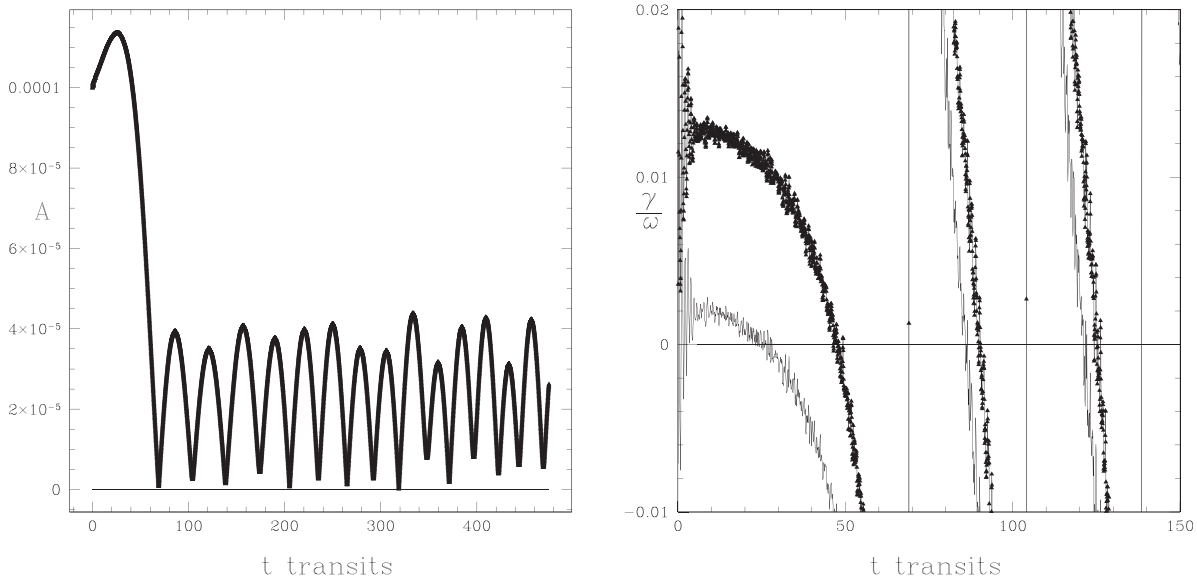

FIG. 3. Time evolution of the mode amplitude and of the growth rate showing strong chirping, 100 kHz. Shown is the growth rate γ/ω as a function of time as well as the value obtained by subtracting the damping, giving the actual amplitude evolution. The time scale in this and later plots is in terms of the toroidal transit time of a characteristic high energy particle.

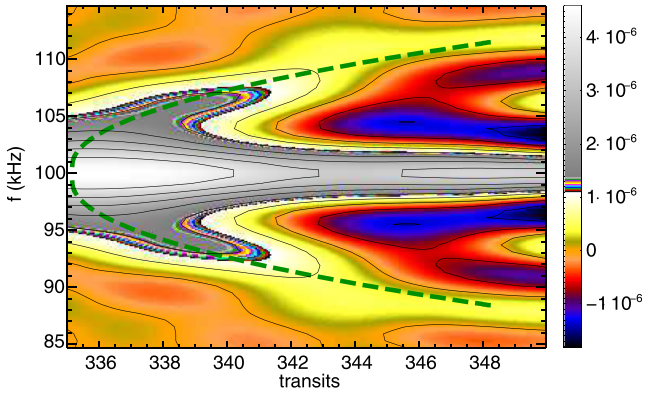

FIG. 4. Time evolution of the frequency spectrum showing strong chirp around 100 kHz, for the same run shown in Fig. 3. The green curve represents the departures $\delta f = \pm\frac{16\sqrt{2}}{\pi^2 3\sqrt{3}}\gamma_L\sqrt{\gamma_d t}$ from the original eigenmode frequency, as the Berk-Briezman prediction.[1] The parameters used for producing this figure were $\gamma_L/\omega = 0.04$, $(\gamma_L - \gamma_d)/\omega = 0.007$, and a toroidal transit time of 4.7μs. The total time in this plot is about 0.1 ms.

present. One can see small delta function phase jumps of $d\phi \simeq 0.01$ at the point in time where the sidebands decrease in the amplitude, at about t = 341 transits in Fig. 4, but nothing stronger than this. Also, it is clear from the plots of the frequency spectrum, such as Fig. 4, that the frequency modulation is slow in time. It has been experimentally verified that the shape of the eigenfunction does not change during the chirp, and the Alfvén mode eigenfunction is the only one present in the simulation. Thus, the chirp must be understood as the strong frequency modulation of a single mode unless one wishes to interpret the clump and hole formation as consisting of independent modes.

In Ref. 1, the wave chirping has been proposed to be associated with self-consistent nonlinear structures that spontaneously move in phase space. The moving resonance allows for a self-organized state in which the extraction of energy occurs in previously unexplored regions of phase space, which can act to overcome background damping. An adiabatic state was analytically explored, in which the mode amplitude is assumed to be roughly preserved during one chirp event. Under this simplification, the frequency excursion has been found to be given by

$$\delta f = \pm\frac{16\sqrt{2}}{\pi^2 3\sqrt{3}}\gamma_L\sqrt{\gamma_d t}. \tag{11}$$

In Fig. 4 is shown a 100 kHz chirp with the square root theoretical time dependence added with dashed lines. Good agreement with the theory is observed although the amplitude drops by about 30% in the period shown.

In Fig. 5 are examples of two chirps. For most cases, we see the sideband frequencies, after separating from the main frequency as $\sqrt{t}$, tracking the main frequency for a significant amount of time. In some cases, as the mode amplitude rebounds from its lowest value, the clump and hole are reabsorbed into the main frequency, as shown in the second case. Occasionally, the chirping does not follow the simple emission of a clump and a hole but shows additional period doubling and branching of the ejected frequencies. Examples are shown in Fig. 6. The first case had an energy drag of 21/s, and the second had none. In Fig. 9, Sec. II B, is shown an experimentally observed example of this compound chirping.

Finally, in Fig. 7 is shown an example of a history of repeated chirping, with significant clump-hole production practically at every amplitude crash.

In Ref. 1, it has been observed that the formation of holes and clumps only occurs when the simulation is started with the mode sufficiently close to its linear marginal stability, more specifically when $\gamma_d \gtrsim 0.4\gamma_L$. More recently, Ref. 6 reported wave chirping occurring regardless of the level of marginality and interpreted the emergence of holes and clumps as arising from negative energy modes at the resonance edges.

Shown in Fig. 8 is the domain in the space of γ_L/ω and γ_d/ω in which chirping is observed in the present simulations, including points obtained from simulations both from this section and also from Sec. II B, using the reversed shear equilibria of NSTX. We find no significant difference in this plot for simulations using different equilibria and mode frequency, and points are included from each of the three cases studied. Empty triangles are cases which did not chirp, solid triangles are normal chirps, and solid squares are cases with complex chirping including subsequent period doubling and a profusion of clumps and holes. There is a threshold for chirping in γ_L/ω of about 0.01, and above this, chirping is observed, provided approximately that $\gamma_d/\gamma_L > 0.2$. For larger values of both γ_L and γ_d, there also occur

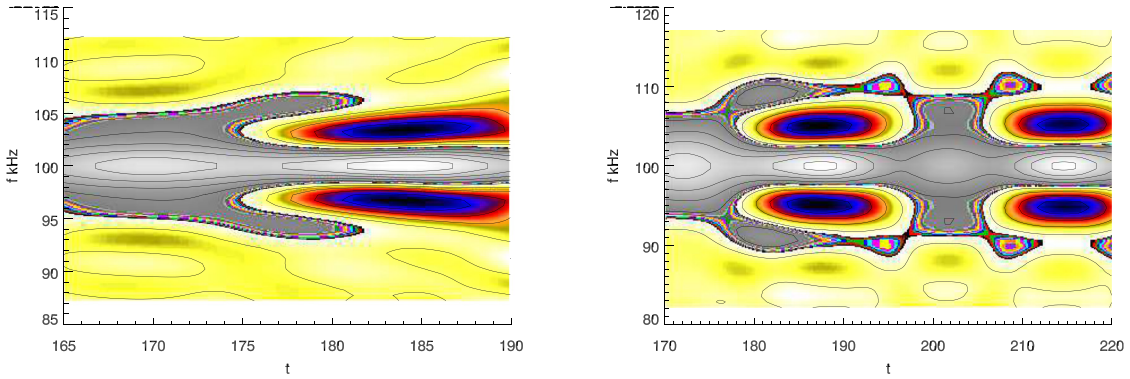

FIG. 5. Time evolution of the frequency spectrum showing strong chirp, 100 kHz, $\gamma_L/\omega = 0.038$, $\gamma_d/\omega = 0.03$, and in the second case, with the subsequent reabsorption of the clump and hole into the main frequency, followed by repeated chirping. The growth rate and damping were $\gamma_L/\omega = 0.035$ and $\gamma_d/\omega = 0.02$.

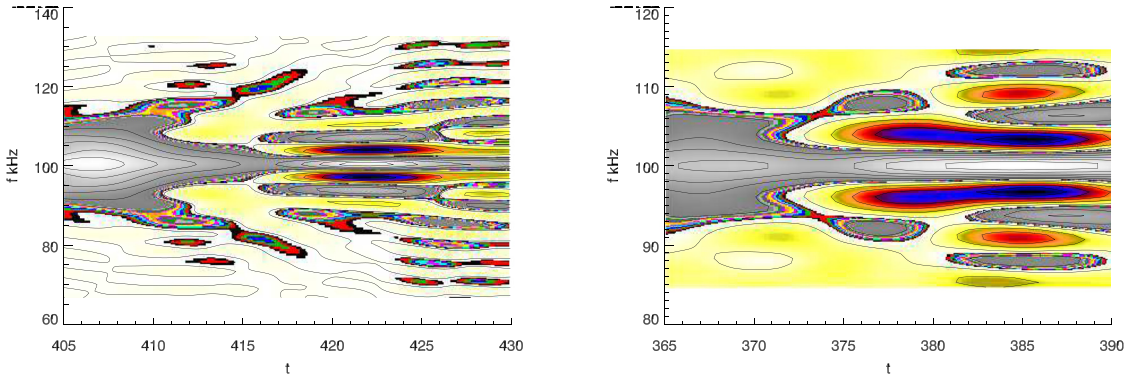

FIG. 6. Time evolution of the frequency spectrum showing strong chirps with secondary doubling, 100 kHz. The growth rate and damping were $\gamma_L/\omega = 0.058$ and $\gamma_d/\omega = 0.053$. The first case had an energy drag of 21/s, and the second had none.

complex chirps, with subsequent frequency doubling and secondary clump emission after the separation of the initial clump and hole, as seen in Fig. 6.

B. NSTX shot 205072

We now examine equilibria and modes associated with particular discharges in NSTX in which chirping was observed. NSTX shot 205072 exhibits a strong chirp at t = 0.36 s. The numerical equilibrium was produced by TRANSP[21] and the mode structure by NOVA.[20] The mode structure is not observed to change appreciably in NSTX during a chirp,[31] which justifies the use of a fixed mode structure throughout the mode nonlinear evolution. The magnetic field on the axis was 6.2 kG. The mode had a toroidal structure of $n = 1$ and poloidal components from $m = 0$, 10. It was a negative frequency mode with $f = -130$ kHz.[32] For this case, we choose a distribution with $\mu B = 2$ keV, and so it is deeply passing.

In Fig. 9 is an experimental plot of the chirp. Note that the mode makes contact with two branches of the continuum at the time of the chirp, indicating possibly a large increase in the value of the mode damping. Because of the small aspect ratio in NSTX, the gap in the continuum closes near the magnetic axis, making the contact with a continuum mode more probable. The experimentally obtained Fourier plot uses the perturbed frequency signal due to the mode and hence also includes, unlike our analysis, the mode amplitude. However, the mode amplitude changes little during the chirp, and in addition, the experimental plot uses a log scale; so the resulting plots are not dissimilar.

In Fig. 10 are shown the equilibrium and q profile. The equilibrium possessed strong reversed shear in the plasma center. In Fig. 11

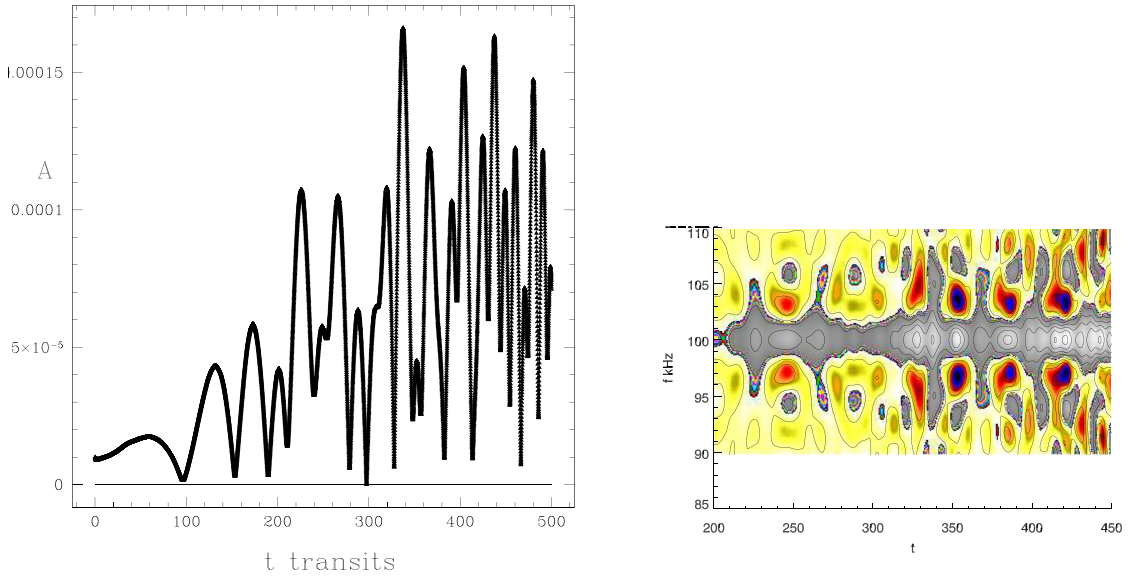

FIG. 7. Time evolution of the mode amplitude and the frequency spectrum with multiple chirps, $f = 100$ kHz; the growth rate and damping were $\gamma_L/\omega = 0.058$ and $\gamma_d/\omega = 0.053$.

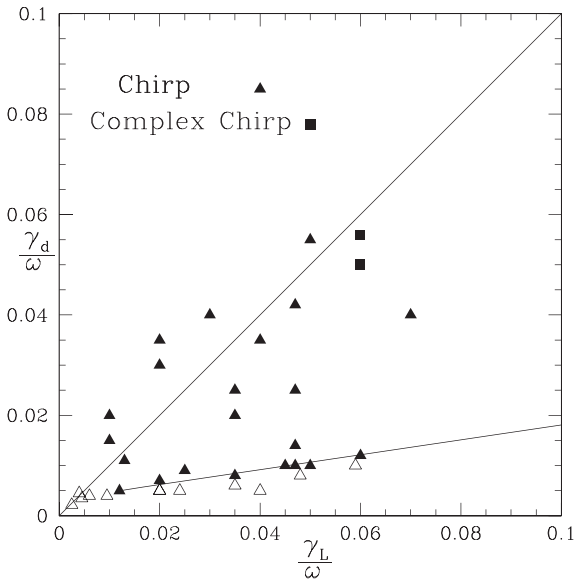

FIG. 8. The domain in which chirping is observed. Empty triangles are simulations in which no chirps were observed, solid triangles are examples of chirping, and solid squares are complex chirps. There is a threshold in γ_L/ω of about 0.01, and after that, chirping is observed, provided approximately that $\gamma_d/\gamma_L > 0.2$.

are shown the determination of the resonance[29,30] in the plane of E and P_ζ for a value of μB of 2 keV and a Poincaré plot of the resonance for a large mode amplitude of $A = 10^{-3}$. The blue line with a large negative slope is the line $\omega P_\zeta - nE = K$, along which the Poincaré plot is made. The mode is produced entirely by the $m = 1$ component of the perturbation, determined by examining Poincaré plots selecting one value of m at a time. It was found that the addition of other harmonics produced no change in the form of the resonance, and so further simulations were made with this poloidal harmonic alone. The radial mode structure is much broader than the resonance width, and so there is no effect on mode evolution due to its width. Also, note that all chirp simulations are limited to small mode amplitudes.

Now, recreation of the situation observed in NSTX is attempted, namely, the sudden chirping of a stable saturated Alfvén mode. As seen in Sec. II A, it is necessary that there is strong damping to produce a significant chirp. We thus hypothesize that the saturated Alfvén mode, due to small changes in the equilibrium, makes contact with the continuum and thus suddenly encounters strong damping. We simulate this by first allowing a mode in the presence of collisions to saturate and then suddenly increase the mode damping. This produces the sequence of events observed in the simulations shown above, with rapid collapse of the mode amplitude and multiple chirps. In Fig. 12 are shown the examples of chirps using this equilibrium.

C. NSTX shot 139048

NSTX shot 139048 exhibits a strong chirp at t = 0.266 s. The equilibrium and q profile were very similar to those shown for shot

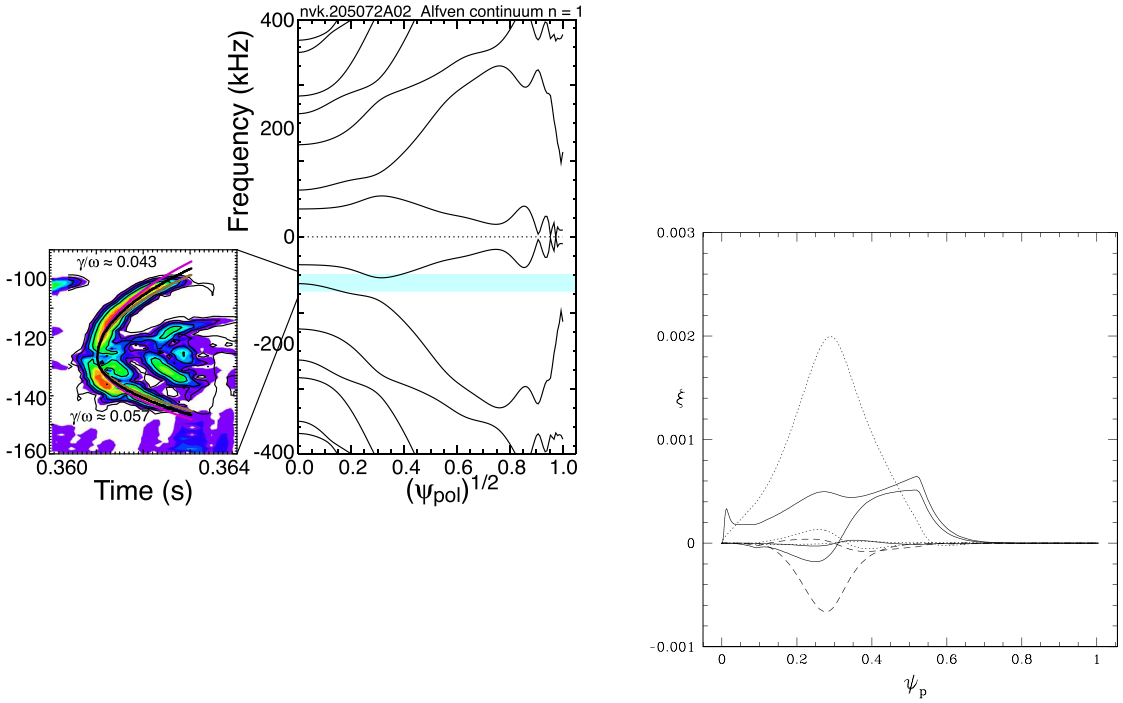

FIG. 9. Chirp observed in NSTX, shot 205072. The mode had a frequency of –130 kHz. The lines on the left frequency plot show continuum modes. The eigenmode, shown at the right, is large near the axis and makes contact with them at two different locations. The clump and hole are fit with Eq. (11) using $\gamma_L/\omega = \gamma_d/\omega$ of 0.043 for the upper branch and 0.057 for the lower branch.

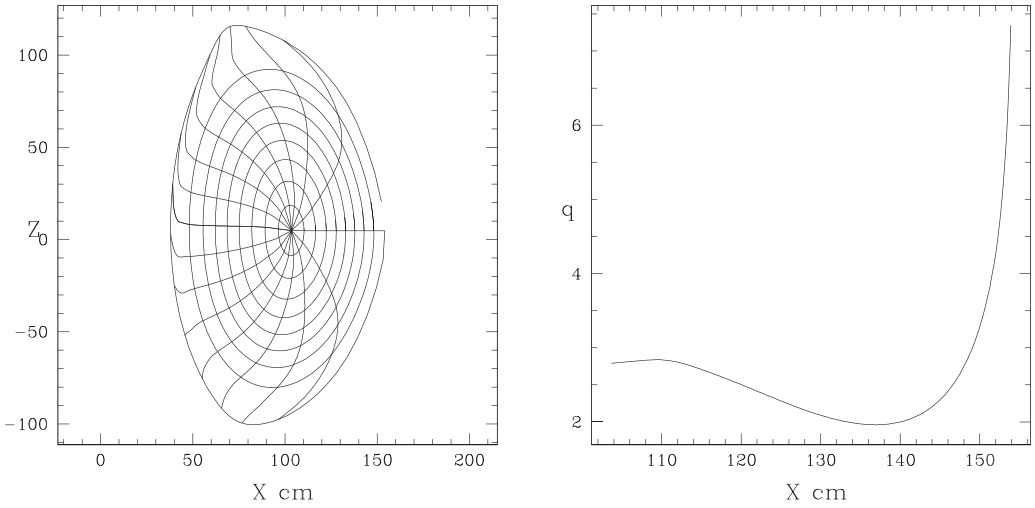

FIG. 10. NSTX equilibrium and q profile, shot 205072.

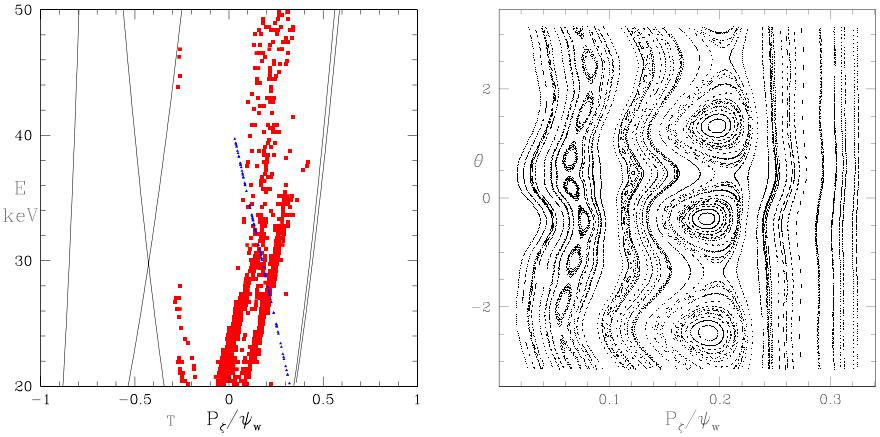

FIG. 11. Resonance determination, NSTX shot 205072, showing the domain in the space of energy and canonical momentum where KAM surfaces are broken, and a Poincaré plot obtained along the line $\omega P_\zeta - nE = K$. The resonance has a poloidal structure of three elliptic points.

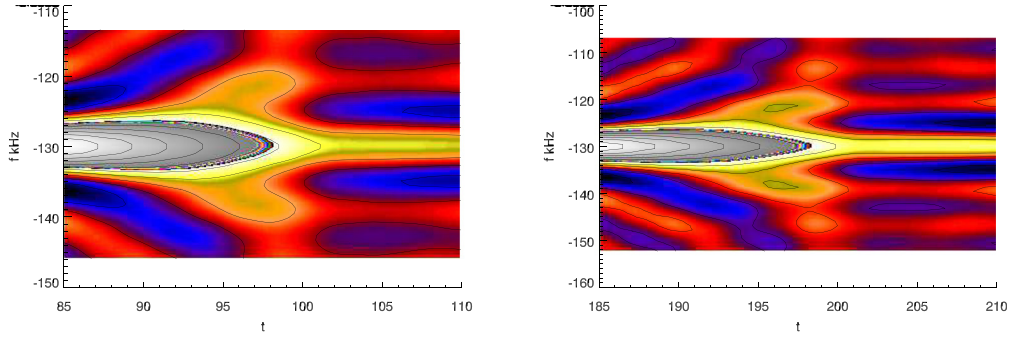

FIG. 12. Examples of simulated chirping using the equilibrium associated with NSTX shot 205072. The growth rate and damping were $\gamma_l/\omega = 0.01$ and $\gamma_d/\omega = 0.02$.

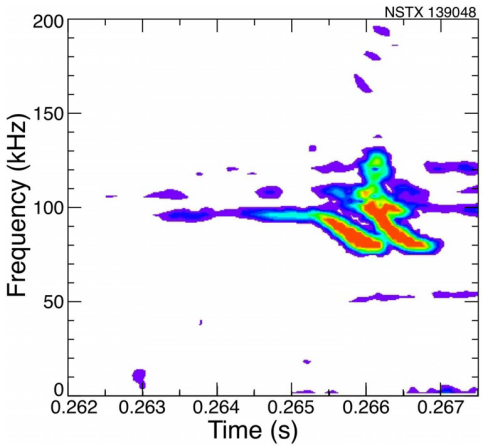

FIG. 13. Chirp observed in NSTX shot 139048.

205072, but the magnetic field was much lower, with $B = 4.9$ kG. The mode had a positive frequency of $f = 100$ kHz. For this case, we chose a distribution with $\mu B = 25$ keV, not as deeply passing as used for shot 205072. The mode is produced entirely by the $m = 1$ component of the perturbation, determined by examining Poincaré plots selecting one value of m at a time. It was found that the addition of other harmonics produced no change in the form of the resonance, and so further simulations were made with this harmonic alone. The radial mode structure is much broader than the resonance width, and so there is no effect on mode evolution due to its width. Unlike shot 205072, the resonance has a poloidal structure of a single elliptic point.

In Fig. 13 is an experimental plot of the chirp. Note that the initial part of the chirp is asymmetric, with the frequency chirping only downward, followed immediately by a more symmetric burst. We have thus far not observed any asymmetric chirping in simulations, possibly due to energy drag, the decreasing kinetic energy of particles in the resonance, or plasma rotation with shear producing the asymmetry.

In Fig. 14 is shown a simulation using the equilibrium of NSTX for shot 139048 and the mode structure provided by NOVA, showing the mode amplitude as a function of time for initiation with no collisions and strong damping. Also shown is the linear growth rate of $\gamma_L/\omega = 0.04$ along with the value including the damping, reducing the growth to about half its value. With no collisions, the mode initially grows until it has exhausted the density gradient with the resonance and then collapses to a small value, and in this process, it produces a chirp, shown in Fig. 15.

A significant collision frequency destroys the coherence of the particles trapped in the resonance and makes chirping impossible. Physically, diffusion acting on the resonant particles destroys the phase-space correlations necessary to sustain coherent chirping structures. This effect was studied in NSTX by employing nonlinear global gyrokinetic simulations.[25]

From analytical theory, it has been shown[33] that solutions of mode evolution near marginality that blows up in a finite time occur when $\nu_{eff}/(\gamma_L - \gamma_d) \lesssim 2$. This explosive behavior signals that the mode is entering a hard nonlinear scenario associated with the emergence of chirping. When scattering collisions are frequent enough, the mode evolves quasisteadily to saturation in the absence of period bifurcation. In this case, the predicted spectral response is oscillation with a constant frequency.

From Eq. (6) of Ref. 34, we have

$$\nu_{eff}^3 \simeq 2\nu_\perp R^2 \left[E\frac{B_{pol}^2}{B^2} + \mu B\right]\left(\frac{\partial \Omega}{\partial P_\zeta}\bigg|_{K,\mu}\right)^2, \tag{12}$$

with $\Omega = n\omega_\zeta - p\omega_\theta$ vs P_ζ for fixed K, where ω_ζ is the mean value of $\Delta\zeta/\Delta t$, ω_θ is the mean value of $\Delta\theta/\Delta t$ for particles launched along the line $K = \omega P_\zeta - nE$, all with $\mu B = 25$ keV, and $p = 1$ is the number of

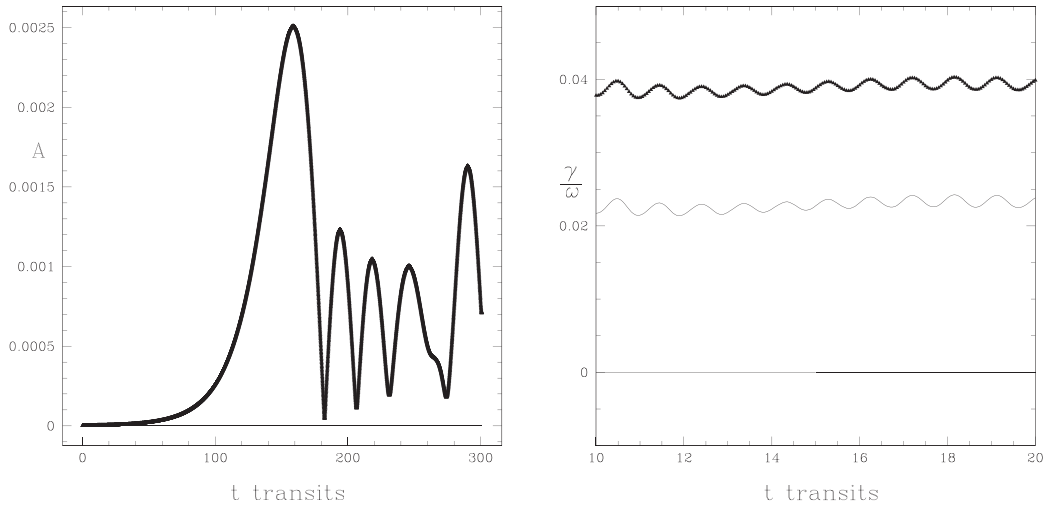

FIG. 14. Simulation of chirping in NSTX shot 139048, which had a mode with a frequency of 100 kHz. Shown is the amplitude and γ_L/ω as well as the value including damping as a function of time. The damping reduces the growth almost to half its linear value.

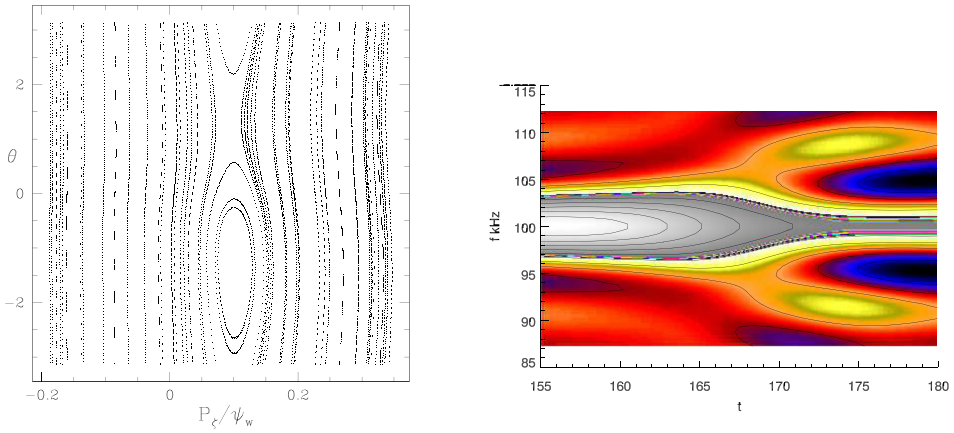

FIG. 15. NSTX shot 139048, mode resonance, and simulation of a Chirp with the initial growth rate and damping as shown in Fig. 14. The growth rate and damping were $\gamma_L/\omega = 0.04$ and $\gamma_d/\omega = 0.018$. Unlike shot 205072, the resonance has a poloidal structure of a single elliptic point.

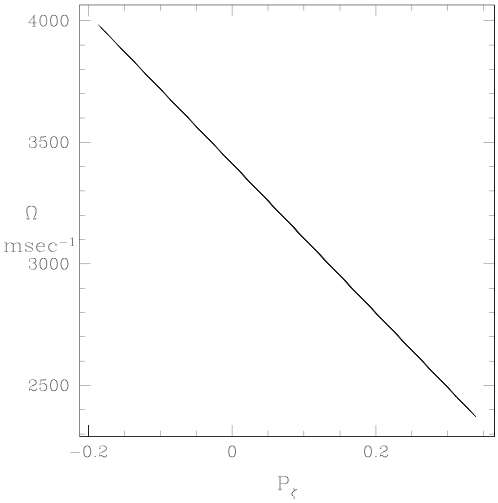

FIG. 16. NSTX shot 139048, $\Omega = n\omega_\zeta - p\omega_\theta$ vs P_ζ for fixed K, and $n = p = 1$. The equilibrium parameters were B = 4.9 kG and $\mu B = 25$ keV.

islands in the resonance. In Fig. 16 is shown a numerical determination of $d\Omega/dP_\zeta$. The canonical momentum P_ζ is in code units.

Figure 17 illustrates the transition between the chirping and the quasisteady oscillation types, induced by extrinsic stochasticity. Figure 17(a) shows the result of collisionless simulation, where the particles are expected to maintain their bounce coherence and, therefore, to lead to wave chirping. In Figs. 17(b) and 17(c), scattering collisions are included. The effective frequency felt by particles at a given resonance is computed via Eq. (10). Panels (b) and (c) used $\nu_\perp = 8.5/s$ and $\nu_\perp = 26/s$, which correspond to $\nu_{eff}/(\gamma_L - \gamma_d) = 2.17$ and $\nu_{eff}/(\gamma_L - \gamma_d) = 3.15$, respectively. While (b) represents a situation where the holes and clumps are barely formed and detached with a minor degree of chirping, (c) shows a situation with fully suppressed chirping structures.

III. CONCLUSION

Multiple examples of classical mode chirping[1] are observed with the guiding center code ORBIT. The essential ingredient is the presence of strong mode damping along with significant drive. The damping must be at least 20% of the linear growth rate, and γ_L/ω must be larger than 0.01. The simulations performed included a numerical equilibrium with a classical q profile quadratic in minor radius as well as the use of NSTX discharges with strongly reversed shear in the core.

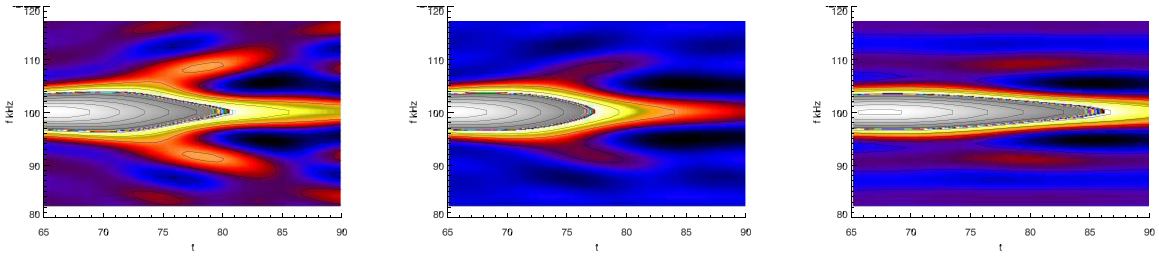

FIG. 17. Effect of collisions using energy conserving pitch angle scattering. A significant collision frequency destroys the coherence of the particles trapped in the resonance and makes chirping impossible. Shown is a chirp with no collisions, with $\nu = 8.5$/s and $\nu = 26$/s. The growth rate and damping were $\gamma_L/\omega = 0.047$ and $\gamma_d/\omega = 0.015$.

No significant change in the conditions necessary for chirping is found using the different equilibria. The shape of the frequency satellites agrees with theory. The necessary strong damping for the production of chirping leads to the conjecture that chirping is caused at least in some cases when small changes in the equilibrium cause a saturated Alfvén mode to come into contact with the continuum and suddenly experience strong damping. Collisions inhibit chirping by destroying the coherence of the particle distribution in the resonance, and the necessary magnitude of the collisions to do this agrees with theory. The poorly understood transition from the chirping to the avalanching regime will be the subject of future investigation.

ACKNOWLEDGMENTS

This work was supported by the U.S. Department of Energy (DOE) under Contract No. DE-AC02-09CH11466.

REFERENCES

[1]H. L. Berk, B. N. Breizman, and N. V. Petviashvili, Phys. Lett. A **234**, 213 (1997).
[2]H. L. Berk, B. N. Breizman, J. Candy, M. Pekker, and V. Petviashvili, Phys. Plasmas **6**, 3102 (1999).
[3]J. Candy, H. L. Berk, B. N. Breizman, and F. Porcelli, Phys. Plasmas **6**, 1822 (1999).
[4]S. D. Pinches, H. L. Berk, D. N. Borba, B. N. Breizman, S. Brigulio, A. Fasoli, G. Fogaccia, M. P. Gryaznevich, V. Kiptily, M. J. Mantsinen *et al.*, Plasma Phys. Controlled Fusion **46**, S47–57 (2004).
[5]M. K. Lilley, B. N. Breizman, and S. E. Sharapov, Phys. Plasmas **17**, 092305 (2010).
[6]M. K. Lilley and R. M. Nyqvist, Phys. Rev. Lett. **112**, 155002 (2014).
[7]J. Lang, G. Y. Fu, and Y. Chen, Phys. Plasmas **17**, 042309 (2010).
[8]X. Wang, S. Brigulio, L. Chen, C. Di Troia, G. Fogaccia, G. Vlad, and F. Zonca, Phys. Rev. E **86**, 045401(R) (2012).
[9]H. Zhang, Z. Lin, and I. Holod, Phys. Rev. Lett. **109**, 025001 (2012).
[10]M. Lesur, Phys. Plasmas **20**, 055905 (2013).
[11]J. Zhu, Z. W. Ma, and G. Y. Fu, Nucl. Fusion **54**, 123020 (2014).
[12]G. Vlad, V. Fusco, S. Brigulio, G. Fogaccia, F. Zonca, and X. Wang, New J. Phys. **18**, 105004 (2016).
[13]A. Bierwage and K. Shinohara, Phys. Plasmas **23**, 042512 (2016).
[14]B. J. Q. Woods, V. N. Duarte, A. J. DeGol, N. N. Gorelenkov, and R. G. L. Vann, Nucl. Fusion **58**, 082015 (2018).
[15]K. G. McClements and E. D. Fredrickson, Plasma Phys. Controlled Fusion **59**, 053001 (2017).
[16]V. N. Duarte, H. L. Berk, N. N. Gorelenkov, W. W. Heidbrink, G. J. Kramer, R. Nazikian, D. C. Pace, M. Podestà, B. J. Tobias, and M. A. V. Zeeland, Nucl. Fusion **57**, 054001 (2017).
[17]E. D. Fredrickson, N. A. Crocker, R. E. Bell, S. S. Darrow, N. N. Gorelenkov, G. J. Kramer, S. Kubota, F. M. Levinson, D. Liu, Ss Medley, M. Podesta, K. Tritz, R. B. White, and H. Yuh, Phys. Plasmas **16**, 122505 (2009).
[18]R. B. White and M. S. Chance, Phys Fluids **27**, 2455 (1984).
[19]S. M. Kaye, M. G. Bell, R. E. Bell, S. Bernabei, J. Bialek, T. Biewer, W. Blanchard, J. Boedo, C. Bush, M. D. Carter *et al.*, Nucl. Fusion **45**, S168–S180 (2005).
[20]C. Z. Cheng and M. S. Chance, Phys. Fluids **29**, 3695 (1986).
[21]A. Pankin, D. McCune, R. Andre, G. Bateman, and A. Kritz, Comput. Phys. Commun. **159**, 157 (2004).
[22]Y. Chen, R. B. White, G.-Y. Fu, and R. Nazikian, Phys. Plasmas **6**, 226 (1999).
[23]R. B. White, N. Gorelenkov, M. Gorelenkova, M. Podesta, S. Ethier, and Y. Chen, Plasma Phys. Controlled Fusion **58**, 115007 (2016).
[24]M. Zhou and R. B. White, Plasma Phys. Controlled Fusion **58**, 125006– 125015 (2016).
[25]V. N. Duarte, N. N. Gorelenkov, M. Schneller, E. D. Fredrickson, M. Podestà, and H. L. Berk, Nucl. Fusion **58**, 082013 (2018).
[26]E. Wigner, Phys. Rev. **40**, 749 (1932).
[27]M. J. Bastiaans, J. Opt. Soc. Am. **69**, 1710 (1979).
[28]A. N. Kolmogorov, Proceedings of the International Congress of Mathematicians (Amsterdam, 1957), Vol. **1**, p. 315; V. I. Arnold, Russ. Math. Surv. **18**(5), 9 (1963); J. Moser, Nachr. Akad. Wiss. Gottingen. II Math. Phys. Kd **1**, 1 (1962).
[29]R. B. White, Commun. Nonlinear Sci. Numer. Simul. **17**, 2200 (2012).
[30]R. B. White, Plasma Phys. Controlled Fusion **53**, 085018 (2011).
[31]M. Podestà, R. Bell, A. Bortolon, N. Crocker, D. Darrow, A. Diallo, E. Fredrickson, G.-Y. Fu, N. Gorelenkov, W. Heidbrink, G. Kramer, S. Kubota, B. LeBlanc, S. Medley, and H. Yuh, Nucl. Fusion **52**, 094001 (2012).
[32]M. Podesta, E. D. Fredricksin, and M. Gorelenkova, Nucl. Fusion **58**, 082023 (2018).
[33]B. N. Breizman, H. L. Berk, M. S. Pekker, F. Porcelli, G. V. Stupakov, and K. L. Wong, Phys. Plasmas **4**, 1559 (1997).
[34]V. N. Duarte, H. L. Berk, N. N. Gorelenkov, W. W. Heidbrink, G. J. Kramer, R. Nazikian, D. C. Pace, M. Podestà, and M. A. Van Zeeland, Phys. Plasmas **24**, 122508 (2017).